PNAS RESEARCH ARTICLE | CELL BIOLOGY OPEN ACCESS

Alternative splicing encodes functional intracellular CD59 isoforms that mediate insulin secretion and are down-regulated in diabetic islets

Ewelina Golec[a], Alexander Ekström[a], Maciej Noga[a], Muhmmad Omar-Hmeadi[b], Per-Eric Lund[b], Bruno O. Villoutreix[c], Ulrika Krus[d], Katarzyna Wozniak[a], Olle Korsgren[e], Erik Renström[d], Sebastian Barg[b], Ben C. King[a,1], and Anna M. Blom[a,1,2]

Edited by Rohit Kulkarni, Joslin Diabetes Center, Boston, MA; received November 3, 2021; accepted April 25, 2022 by Editorial Board Member C. Ronald Kahn

Human pancreatic islets highly express CD59, which is a glycosylphosphatidylinositol (GPI)-anchored cell-surface protein and is required for insulin secretion. How cell-surface CD59 could interact with intracellular exocytotic machinery has so far not been described. We now demonstrate the existence of CD59 splice variants in human pancreatic islets, which have unique C-terminal domains replacing the GPI-anchoring signal sequence. These isoforms are found in the cytosol of β-cells, interact with SNARE proteins VAMP2 and SNAP25, colocalize with insulin granules, and rescue insulin secretion in CD59-knockout (KO) cells. We therefore named these isoforms IRIS-1 and IRIS-2 (Isoforms Rescuing Insulin Secretion 1 and 2). Antibodies raised against each isoform revealed that expression of both IRIS-1 and IRIS-2 is significantly lower in islets isolated from human type 2 diabetes (T2D) patients, as compared to healthy controls. Further, glucotoxicity induced in primary, healthy human islets led to a significant decrease of IRIS-1 expression, suggesting that hyperglycemia (raised glucose levels) and subsequent decreased IRIS-1 expression may contribute to relative insulin deficiency in T2D patients. Similar isoforms were also identified in the mouse CD59B gene, and targeted CRISPR/Cas9-mediated knockout showed that these intracellular isoforms, but not canonical CD59B, are involved in insulin secretion from mouse β-cells. Mouse IRIS-2 is also down-regulated in diabetic db/db mouse islets. These findings establish the endogenous existence of previously undescribed non–GPI-anchored intracellular isoforms of human CD59 and mouse CD59B, which are required for normal insulin secretion.

type 2 diabetes | insulin secretion | CD59 | SNAREs | intracellular complement

Significance

This project describes the existence of previously unknown non–GPI-anchored CD59 isoforms required for insulin secretion, named CD59–IRIS-1 and CD59–IRIS-2, and finds reduced expression of CD59-IRIS isoforms in human diabetic islets, showing a link between dysregulation of IRIS isoforms and defects in insulin secretion in diabetic patients. These data open a path for future studies into CD59-IRIS expression and function in additional cell types capable of regulated secretion. Identification of additional specific CD59-IRIS binding partners within the cell could provide therapeutic targets for enhancement of insulin secretion in T2D.

Type 2 diabetes (T2D) is a metabolic disorder characterized by persistent hyperglycemia due to insufficient insulin secretion unable to compensate for insulin resistance in peripheral tissues. Complement proteins are components of innate immunity, responsible for host defense and inflammation (1, 2); however, the complement system also contributes to T2D, which develops after years of prediabetes during which increased glucose levels (glucotoxicity), as well as oxidative, metabolic, and inflammatory stress impair insulin secretion (3, 4). Pancreatic islets are richly vascularized and constantly exposed to high concentrations of serum complement proteins; therefore, protection of islets from complement-mediated damage is necessary. Such protection is served by CD59, a ubiquitously expressed, glycosylphosphatidylinositol (GPI)-anchored cell surface protein, that inhibits formation of the complement membrane attack complex (5), a multimeric pore-forming complex of complement proteins that breaches lipid membranes. We previously found that the complement inhibitor CD59 was highly expressed in pancreatic islets (6). Unexpectedly, CD59 knockdown in a rat β-cell line strongly suppressed glucose-stimulated insulin secretion (GSIS). Enzymatic removal of cell-surface CD59 did not affect insulin secretion, leading to the conclusion that an intracellular pool of CD59 was involved in insulin secretion. In β-cells with CRISPR/Cas9-mediated knockout of GPI-anchor synthesis, GSIS still occurred but was CD59 dependent (7), implying involvement of non–GPI-anchored CD59 in insulin secretion. However, this previous data did not identify how endogenous forms of non–GPI-anchored CD59 are produced in β-cells. In the current study we discovered human and mouse CD59 splice variants with alternative C-terminal domains in place of the GPI-anchoring site. Both isoforms are found in primary pancreatic islets and rescue insulin secretion when transfected into CD59 knockout (KO) cells. We named these isoforms IRIS-1 and IRIS-2 (Isoforms Rescuing Insulin Secretion 1 and 2). Our data prove the existence of previously undescribed non–GPI-anchored isoforms of CD59 in human and mouse and demonstrate their involvement in the molecular machinery of

Author contributions: E.G., E.R., S.B., B.C.K., and A.M.B. designed research; E.G., A.E., M.N., M.O.-H., P.-E.L., B.O.V., and K.W. performed research; U.K., O.K., and S.B. contributed new reagents/analytic tools; E.G., A.E., M.N., M.O.-H., P.-E.L., B.O.V., U.K., K.W., O.K., E.R., S.B., and B.C.K. analyzed data; and E.G., B.O.V., B.C.K., and A.M.B. wrote the paper.

The authors declare no competing interest.

This article is a PNAS Direct Submission. R.N.K. is a guest editor invited by the Editorial Board.

Copyright © 2022 the Author(s). Published by PNAS. This open access article is distributed under Creative Commons Attribution-NonCommercial-NoDerivatives License 4.0 (CC BY-NC-ND).

[1]B.C.K. and A.M.B. contributed equally to the work.

[2]To whom correspondence may be addressed. Email: anna.blom@med.lu.se.

This article contains supporting information online at http://www.pnas.org/lookup/suppl/doi:10.1073/pnas.2120083119/-/DCSupplemental.

Published June 6, 2022.

Downloaded from https://www.pnas.org by Uppsala Universitetsbibliotek on September 22, 2022 from IP address 130.238.191.184.

β-cell exocytosis. Moreover, a lack of or decreased expression of IRIS isoforms may be involved in the development of T2D.

Results

Characterization of Human IRIS-1 and IRIS-2. In our previously published paper, we showed that artificially created mutants of CD59 lacking the GPI anchor are able to rescue insulin secretion in CD59-knockout β-cells (7). However, these previous data did not identify how endogenous forms of non–GPI-anchored CD59 are produced in β-cells. To answer this question, we analyzed available total RNA transcriptome sequencing data from human pancreatic islets, where we searched specifically for novel splice forms of CD59 lacking the GPI anchor. RNA sequencing (RNA-seq) revealed the presence of two alternative splice forms of human CD59, which lack the GPI-anchoring domain and have novel C-terminal domains (Fig. 1*A*). These isoforms were named: IRIS-1 and IRIS-2 (Isoforms Rescuing Insulin Secretion 1 and 2). IRIS-1 (Ref. No. ENST00000534312.5) lacks the canonical exon 4 encoding the GPI-anchor signal sequence. An additional 3′ exon encoding the C-terminal domain of IRIS-1 is instead derived from the adjacent uncharacterized predicted open reading frame C11orf91, which has an evolutionarily conserved position adjacent to the CD59 gene. IRIS-2 (Ref. No. ENST00000643183.1) in contrast, has an additional exon inserted between canonical exons 3 and 4, causing a frameshift at the C terminus; therefore, IRIS-2 has about 47 % similarity to canonical CD59, and is also not GPI anchored. To gain additional knowledge about these proteins, we modeled the three-dimensional (3D) structures of human IRIS-1 and IRIS-2. The 3D structure of human CD59 is mainly composed of three β-sheets and an α-helix (Fig. 1*B*) (Protein Data Bank [PDB] file: 2j8b) (5). It displays a single N-linked glycosylation site at Asn18 and is stabilized by five disulfide bridges. IRIS-1 is also expected to adopt the 3D fold of CD59, and five disulfide bridges are still present (Fig. 1*C*), consistent with the LU domain structure of the Ly-6/uPAR family of proteins to which CD59 belongs. The C-terminal region of IRIS-1 (28 residues) is missing in the experimental template but is predicted to form a helical structure. This helix could pack against the remaining part of the protein or adopt a more open conformation. Alternatively, the C-terminal domain may remain disordered, but could adopt a helical conformation when in contact with binding partners. This partially disordered region was predicted to be a potential protein–protein or protein–DNA interaction site. The predicted 3D structure of IRIS-2 superimposed onto the human CD59 experimental structure is seen in Fig. 1*D*. This tertiary structure of canonical CD59 is partially conserved, but with an extended flexible loop between β-strands C and D. PCR primers were designed to specifically detect canonical CD59, IRIS-1, and IRIS-2. Both IRIS-1 and IRIS-2 were detected at the RNA level in isolated human pancreatic islets (Fig. 1*E*), but not in RNA from human liver, suggesting tissue-specific expression of IRIS isoforms. The expression of IRIS-1 and -2 was then assessed in various human tissues, revealing wide expression, with the highest levels found in pancreatic islets and placenta (Fig. 1*F* and *SI Appendix*, Fig. S1*A*). We next aimed to verify human IRIS-1/2 expression at the protein level. For this purpose, rabbit antibodies were generated against the unique C-terminal peptides that are present in the isoforms, but not in canonical CD59. Antibody specificity and sensitivity were verified using INS-1 cells overexpressing FLAG-tagged cDNA constructs of IRIS-1 and IRIS-2, recombinant human IRIS-1 and IRIS-2 proteins, and blocking of the IRIS antibodies with peptide antigens used for the generation of the antibodies (*SI Appendix*, Fig. S1*B* and S3–S5). Immunofluorescent staining of dispersed (Fig. 1*G*) and intact primary human pancreatic islets (*SI Appendix*, Fig. S1*D*) revealed an intracellular location of both isoforms, as well as colocalization with insulin granules. Both isoforms are present in β-, but also in α-cells, as demonstrated by colocalization with both insulin and glucagon (*SI Appendix*, Fig. S1*D*). In addition to the cytoplasmic localization, IRIS-1 also had a nuclear localization in a subset of β-cells.

IRIS-1 and IRIS-2 Regulate Insulin Secretion and Are Down-Regulated in Diabetic Islets and by Glucose Exposure. To investigate the functional relevance of IRIS-1 and IRIS-2 in pancreatic β-cells, we expressed FLAG-tagged cDNA constructs of the human CD59-IRIS in the rat INS-1 β-cell line in which CD59 was knocked out using CRISPR/Cas9. Transmission electron microscopy with immunogold labeling for IRIS-1 or IRIS-2 (20 nm gold particles), and insulin (10 nm gold particles), showed that the level of colocalization between IRIS isoforms and insulin granules increased in high glucose conditions, consistent with CD59-IRIS isoforms being involved in insulin secretion (Fig. 2 *A* and *B*, quantified in Fig. 2*C*). Interestingly, glucotoxicity induction in primary, healthy human islets significantly decreased IRIS-1 expression at the protein levels (Fig. 2*D*). Further, we also found that IRIS-1 was down-regulated in primary human islets from T2D patients, as compared to healthy controls (Fig. 2*E*, quantified in Fig. 2*F*). Intriguingly, the apparent molecular weight of IRIS-1 is lower in human islets than that of IRIS-1 expressed in INS-1 cells. Treatment of INS-1 cell lysates with deglycosylating enzymes led to a shift in IRIS-1 apparent mass to that present in human islets (Fig. 2*E*), suggesting a difference in glycosylation status of this isoform in rat and human cells. We also detected a significant decrease in protein level of IRIS-2 in T2D donor islets (Fig. 2*G*, quantified in Fig. 2*H*). Our data suggest that hyperglycemia (raised blood glucose levels) may be one of the factors resulting in decreased IRIS-1/2 expression in T2D patients.

Insulin Secretion Is Rescued by IRIS-1 and IRIS-2 in CD59 Knockout Cells, with Different Insulin Release Kinetics. We next investigated whether IRIS-1/2 isoform introduction into INS-1 CD59 knockout (KO) cells was able to rescue insulin secretion. Knockout of endogenous CD59 strongly inhibits GSIS in INS-1 cells, but reexpression of both canonical CD59 (wild type [WT]) or IRIS-1 or IRIS-2 reversed this loss of GSIS (Fig. 3*A*). We next tested secretion in CD59-KO cells transfected with IRIS isoforms in the presence of diazoxide, which prevents spontaneous depolarization of the cell membrane by opening ATP-sensitive potassium channels and inhibition of calcium influx through voltage-gated channels. In the absence of diazoxide, stimulation with high glucose significantly increased insulin secretion in IRIS-1– and IRIS-2–expressing cells, as compared to CD59-KO. In the presence of diazoxide, we observed an increase in potassium-stimulated insulin secretion in cells overexpressing IRIS isoforms, but not in CD59-KO (Fig. 3*B*). IRIS-mediated rescue of secretion in CD59-KO INS-1 cells was also confirmed by live cell imaging of fluorescently labeled granule exocytosis by total internal reflection microscopy (TIRF) (Fig. 3*C*), as well as by single-cell patch-clamp capacitance measurements of exocytosis in response to a train of depolarizations (Fig. 3 *D* and *E*). Further, to check whether insulin secretion is altered in the human β-cell line (EndoC-βH1) when total human CD59 is knocked down, we performed an insulin secretion assay on EndoC-βH1 cells transfected with siRNA against human CD59 or nontargeting negative control. Knockdown of CD59 strongly inhibits insulin

Downloaded from https://www.pnas.org by Uppsala Universitetsbibliotek on September 22, 2022 from IP address 130.238.191.184.

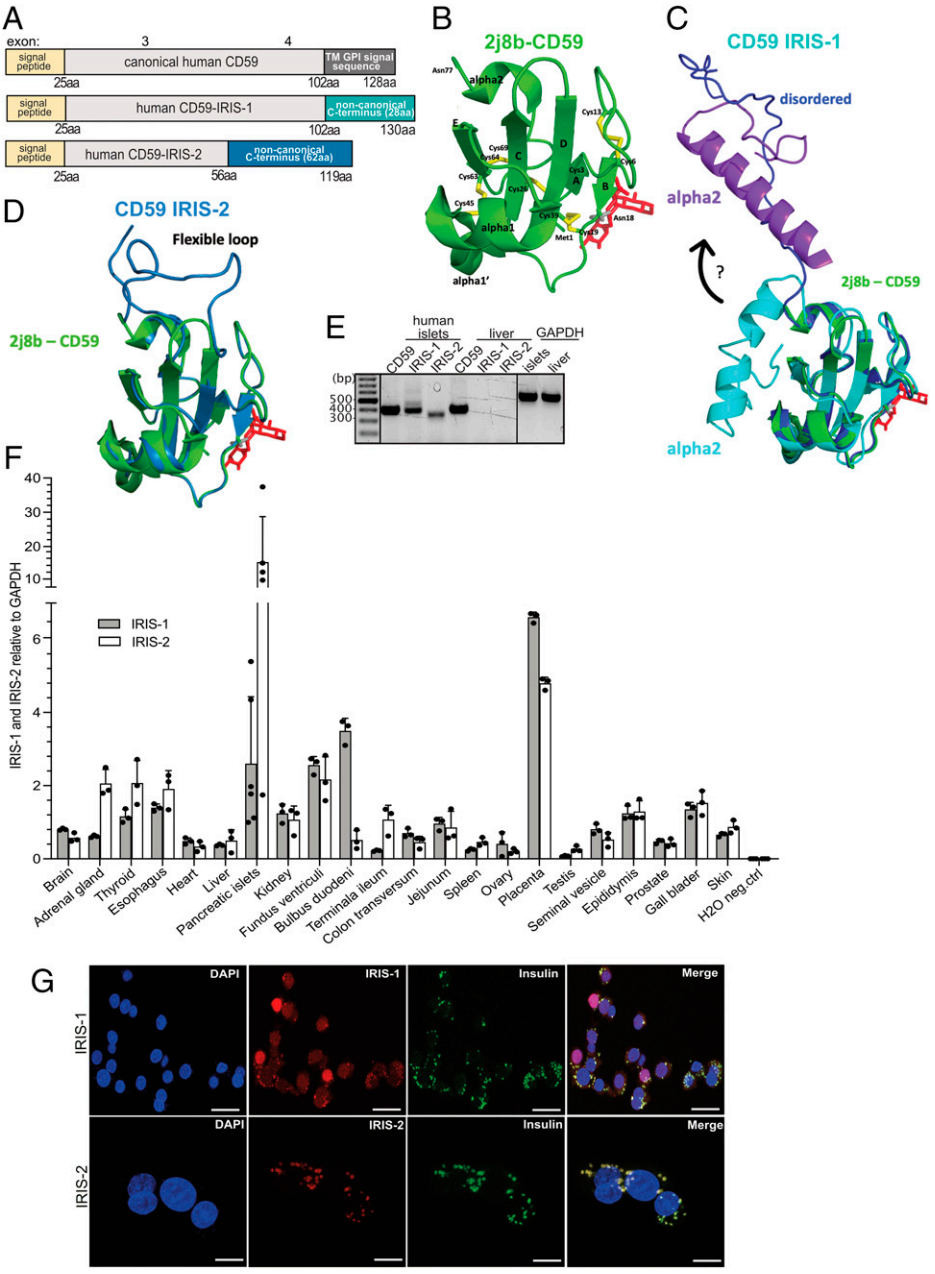

Fig. 1. (*A*) Scheme representing the two alternative splice forms of human CD59, which lack the GPI-anchoring domain and have C-terminal domains. (*B*) The 3D structure of human CD59 is shown with the secondary structure elements labeled and the five-disulfide bonds displayed (yellow). The *N*-glycan at Asn18 is marked in red. (*C*) Predicted structure of human IRIS-1 (cyan) superimposed onto canonical CD59. The C-terminal region of IRIS-1 (the last 28 residues) is missing in the experimental template and predicted to have different conformations: a helical structure (in cyan) packing against the remaining part of the protein, a more open conformation (in purple), or the C-terminal sequence of IRIS-1 is disordered (in dark blue) but could adopt a helical conformation when in contact with other macromolecules. (*D*) Predicted structure of human IRIS-2 (blue) superimposed onto canonical CD59. The predicted longer loop of IRIS-2 is flexible (blue). One disulfide bond, equivalent to C64–C69 of canonical human CD59 is missing due to C-terminal amino acid changes in IRIS-2. (*E*) Expression of CD59 isoforms: IRIS-1, IRIS-2, and canonical CD59 in human pancreatic islets and liver, RNA level. RT-PCR, $n = 3$, biological repeats. (*F*) Expression of IRIS-1 and IRIS-2 (relative to glyceraldehyde 3-phosphate dehydrogenase (GAPDH)) in various human tissues was measured by RT-PCR, $n = 3$ technical repeats. (*G*) Staining with specific antibodies against IRIS-1 or IRIS-2 (red) in dispersed, primary human pancreatic islets, and colocalization with insulin granules . Nuclei stained with DAPI (blue). Results are representative for donor #317 and were repeated with human pancreatic islets from three different healthy donors.

exocytosis, as shown in Fig. 3*F* and *SI Appendix*, Fig. S1*C*. Elevated glucose elicits a biphasic insulin release, with a first rapid exocytosis of readily releasable granules lasting about 10 min, followed by a second phase of pulsatile, slowly developing release as reserve pools of granules are mobilized to the cell surface. Therefore, we hypothesized that the two IRIS isoforms will regulate different phases of insulin release. GSIS in IRIS-1–expressing CD59-KO INS-1 cells occurred within the rapid phase of the first 12 min, in contrast to IRIS-2–expressing cells, where initial secretion was slow but increased further within 12 to 60 min (Fig. 3*G*). This suggests that IRIS-1 affects the readily releasable pool of insulin granules secreted during the first phase of secretion, whereas IRIS-2 is involved in the second phase of release. To investigate other potential effects of CD59-IRIS on the triggering pathway of exocytosis, we quantified ion channel currents by patch-clamp electrophysiology in CD59-KO cells and in CD59-KO cells stably overexpressing IRIS-1 or IRIS-2. The knockout cells had Ca^{2+} and Na^{+} currents with voltage dependencies similar to those in control INS-1 cells. However, the Ca^{2+} current amplitude was

Downloaded from https://www.pnas.org by Uppsala Universitetsbibliotek on September 22, 2022 from IP address 130.238.191.184.

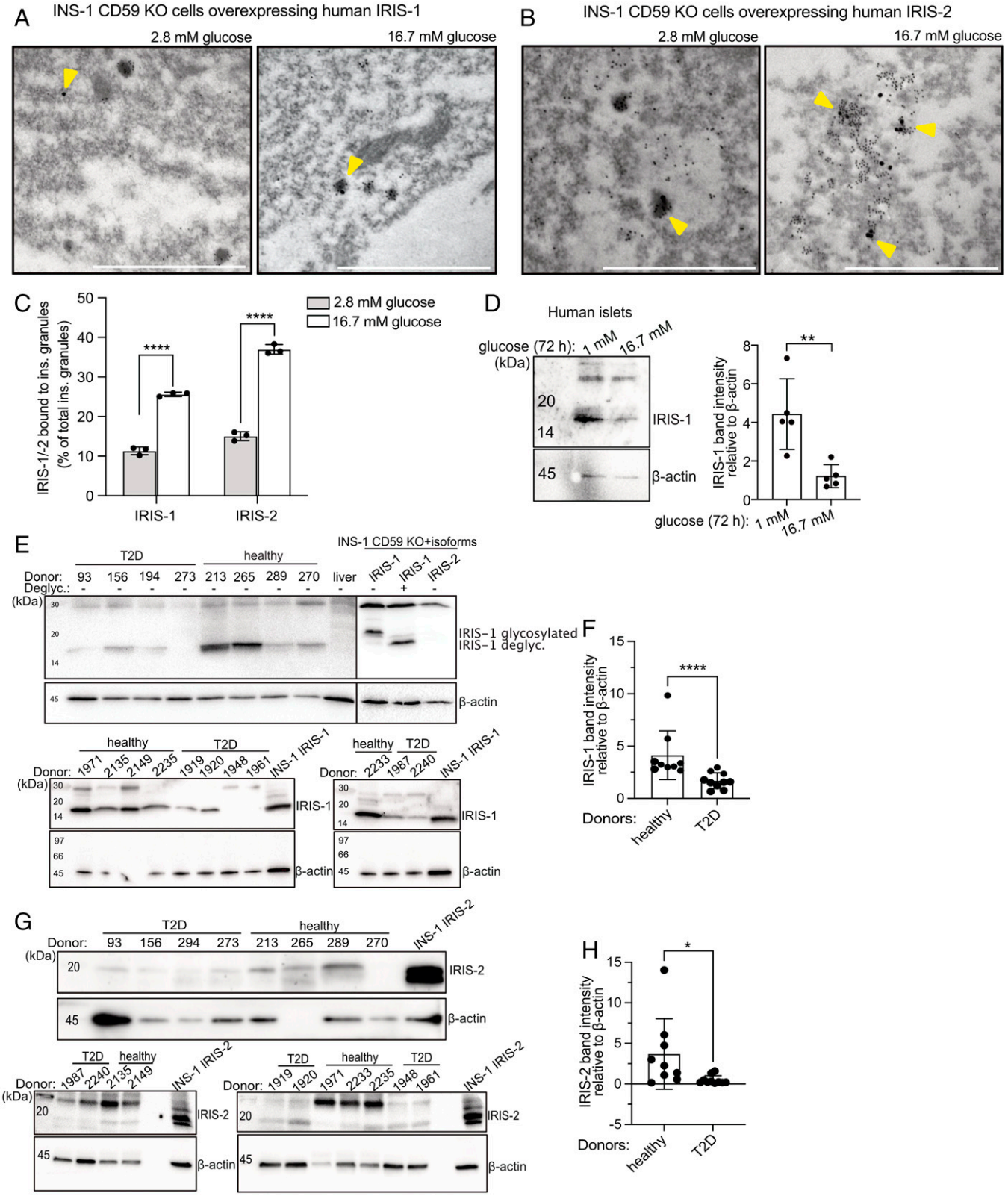

Fig. 2. (*A* and *B*) Transmission electron microscopy with immunogold-labeled IRIS-1 (*A*), and IRIS-2 (*B*) antibodies (20-nm particles) and insulin antibodies (10-nm particles) were used to visualize the binding between IRIS-1/2 and insulin granules in INS-1 CD59-knockout (KO) cells overexpressing human IRIS-1 or IRIS-2, after low or high glucose incubation. Colocalization between IRIS proteins and insulin granules in low and high glucose conditions was quantified in *C*. (*D*) Isolated healthy human pancreatic islets were divided into two and treated with either low (1 mM), or high (16.7 mM) glucose for 72 h, followed by blotting using specific IRIS-1 antibodies. Quantification of five biological repeats (five different donors) is shown on the *Right*. (*E*) IRIS-1 protein levels were assessed by blotting of human pancreatic islets from T2D and healthy donors. Quantification of three technical repeats from nine healthy and 10 T2D donors is shown in *F*. Lysates of INS-1 cells overexpressing CD59 isoforms, treated with deglycosylating enzymes, indicates lack of glycosylation of IRIS-1 in human pancreatic islets and specificity of the IRIS-1 antibody. (*G*) IRIS-2 protein levels were assessed by blotting of human pancreatic islets from T2D and healthy donors. Quantification of three technical repeats from nine healhy and 10 T2D donors is shown in *H*. Statistics (in *C*): two-way ANOVA with Bonferroni's posttest; (in *D*): two-tailed, paired *t* test; (in *F* and *H*): nonparametric Mann–Whitney test. Error bars indicate SD. **P* < 0.05, ***P* < 0.01, and *****P* < 0.0001.

Downloaded from https://www.pnas.org by Uppsala Universitetsbibliotek on September 22, 2022 from IP address 130.238.191.184.

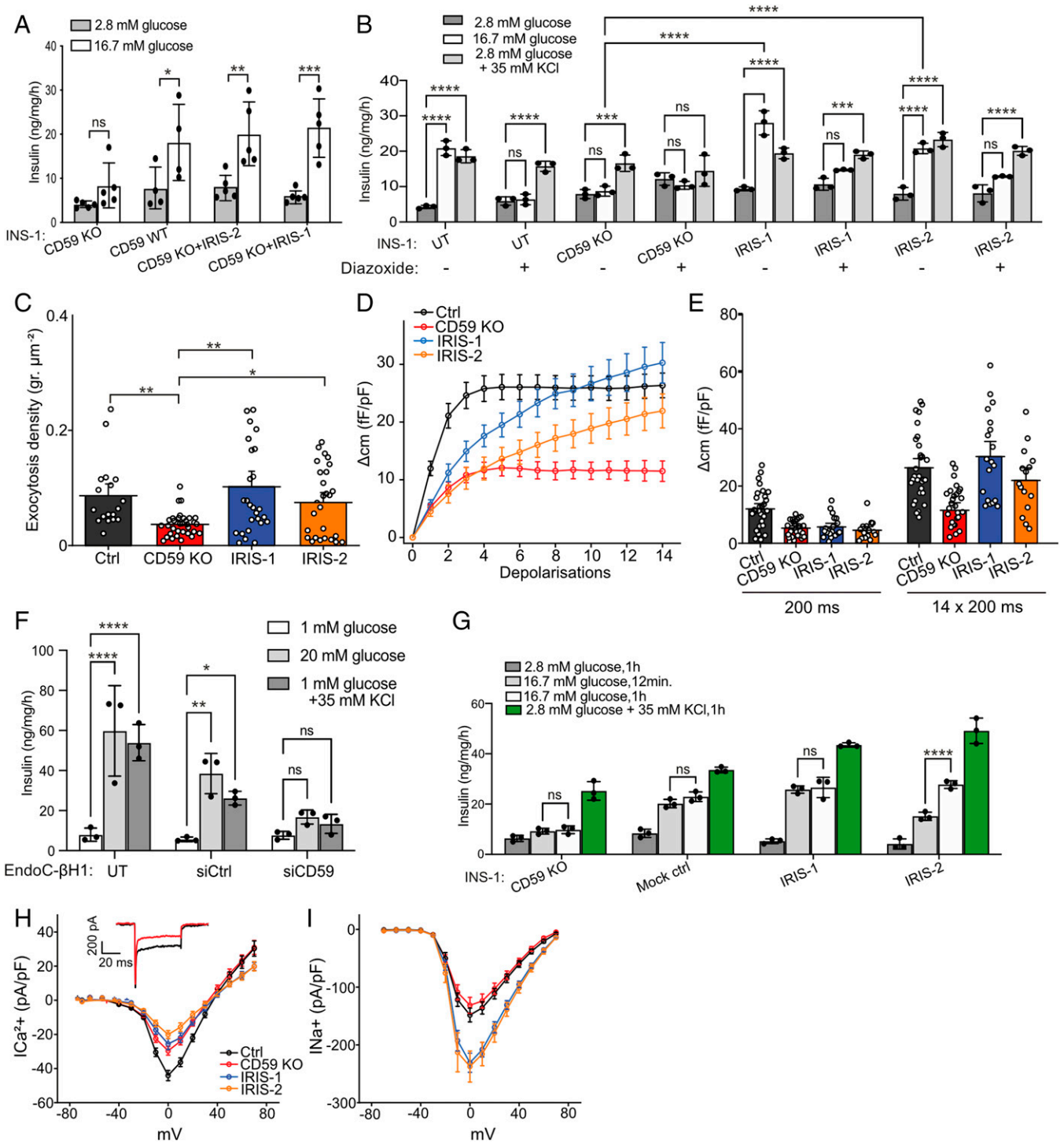

Fig. 3. (*A*) GSIS was carried out in INS-1 CD59-KO cells transfected (transient transfection) with WT CD59, IRIS-1, or IRIS-2; $n = 5$. Each data point represents the average of three independent repeats for five different CD59-KO clones (untransfected [UT] or transfected with human CD59-WT, or IRIS-1, or IRIS-2). (*B*) GSIS (16.7 mM glucose in the presence of 200 µM diazoxide) carried out in mock control and INS-1 CD59-KO cells transiently expressing IRIS-1 and IRIS-2; $n = 3$ biological repeats. (*C*) Exocytosis by TIRF-M: Total K^+ depolarization induced exocytosis during 40 s in control INS-1 cells (black, $n = 18$ cells, three preparations), CD59-KO cells (red, $n = 33$ cells, three preparations), and CD59-KO cells stably overexpressing IRIS-1 (blue, $n = 27$ cells, three preparations) or IRIS-2 (orange, $n = 27$ cells, three preparations). (*D*) Exocytosis by patch clamp: Average cell capacitance time course (ΔCm, ±SEM) during a train of 14 × 200-ms depolarizations from −70 mV to 0 mV ($n = 15$, 30 cells assessed per clone). (*E*) Average changes in membrane capacitance from *H*, during the first depolarization, and total increase during the train of 14 depolarizations. (*F*) GSIS was carried out in EndoC-βH1 cells UT or transfected with siRNA against total human CD59 (siCD59) or negative control (siCtrl). $n = 3$ biological repeats. (*G*) GSIS inducing first (12 min) and second (1 h) phase of insulin exocytosis carried out in INS-1 CD59-KO cells stably overexpressing IRIS-1 and IRIS-2; $n = 3$, biological repeats. (*H* and *I*) Current–voltage relationship of inward currents in control INS-1 cells (black, $n = 30$ cells, four preparations), CD59-KO cells (red, $n = 29$ cells, four preparations), and CD59-KO cells stably overexpressing IRIS-1 (blue, $n = 19$ cells, three preparations) or IRIS-2 (orange, $n = 15$ cells, three preparations). (*H*) Average Ca^{2+} current during 5 to 45 ms of the depolarization and (*I*) peak Na^+ current during the first 5 ms of the depolarization ($p = 0.0001$ for IRIS-1 and 0.001 for IRIS-2 vs. CD59-KO). Statistics (in *A*, *B*, and *F*): two-way ANOVA with Bonferroni's posttest, (in *C*): one-way ANOVA with Fisher's posttest, (in *D*, *E*, *H*, and *I*): two-tailed, unpaired *t* test. (in *G*): two-way ANOVA with Dunnett's posttest. Error bars indicate SD. $^*P < 0.05$, $^{**}P < 0.01$, $^{***}P < 0.001$, and $^{****}P < 0.0001$.

Downloaded from https://www.pnas.org by Uppsala Universitetsbibliotek on September 22, 2022 from IP address 130.238.191.184.

decreased by half in CD59-KO cells, regardless of IRIS reintroduction, when compared with INS-1 control cells (Fig. 3*H*), and the Na^+ current was doubled in cells expressing either IRIS-1 or IRIS-2 (Fig. 3*I*). Taken together, the data support the notion that IRIS isoforms directly affect the exocytosis machinery.

IRIS-1 and IRIS-2 Interact with SNARE Proteins. A vital step in insulin secretion is formation of ternary complexes of soluble *N*-ethylmaleimide-sensitive factor attachment protein receptor (SNARE) proteins, composed of Syntaxin-1A, SNAP25, and vesicle-associated membrane protein (VAMP2) in a 1:1:1 ratio, which fuses the insulin granule with the plasma membrane. These SNARE proteins are found in or associated with the cell or insulin granule membrane, facing the cytosol. IRIS-1 and IRIS-2 expressed in INS-1 CD59-KO cells were also found in both cytosolic and membrane and organelle fractions, as shown by Western blot of subfractionated cells (Fig. 4*A*). Control proteins were found in expected compartments. We found an interaction between IRIS-1, IRIS-2, and overexpressed canonical CD59, with VAMP2 by coimmunoprecipitation (Fig. 4*B*), implicating their association with the exocytotic machinery. The interaction between IRIS isoforms and both VAMP2 and SNAP25 was further verified by enzyme-linked immunosorbent assay (ELISA) (Fig. 4 *C* and *D*) and proximity ligation assay (Fig. 4*E*, quantified in Fig. 4*F*). In addition, the interactions between IRIS isoforms and SNARE proteins increased significantly upon stimulation with high glucose. High glucose concentrations cause the closure of ATP-sensitive potassium channels, membrane depolarization, and opening of voltage-gated calcium channels. Open calcium channels allow for calcium influx and raise its intracellular concentration, which triggers the fusion of insulin granules with the plasma membrane and insulin release. In order to test whether changes in intracellular calcium levels will alter CD59-SNARE binding, the cell-permeable calcium chelator, BAPTA-AM was used. We did not observe any differences in binding between IRIS-1/2 and the vesicle-associated protein VAMP2. However, the binding of IRIS proteins to SNAP25 was partially but significantly diminished when calcium was chelated (Fig. 4*E*, quantified in Fig. 4*F*).

Non–GPI-Anchored Isoforms of Mouse CD59B Contribute to Insulin Secretion in Mice. We also investigated whether similar CD59 isoforms exist in other species. We identified two non–GPI-anchored CD59 splice isoforms in mouse *Cd59b*, which we named CD59B–IRIS-1 and –IRIS-2. In mice, the *Cd59* gene has undergone duplication, resulting in *Cd59a* and *Cd59b*, with the splice forms being present only in *Cd59b* (Fig. 5*A*). Compared to the ubiquitous expression pattern of *CD59a*, mouse *CD59b* has limited tissue-specific expression (8), including pancreatic islets (6), suggesting a specialized function. We modeled the 3D structures of the mouse CD59B-IRIS isoforms. Mouse CD59B–IRIS-1 (Fig. 5*B*) is smaller than human CD59, with about 45 % sequence identity with the experimental template and only two of five disulfide bonds retained. The mouse IRIS-2 model (Fig. 5*C*) has only three disulfide bonds conserved compared to canonical CD59. Molecular simulation predicts that the C-terminal domain of mouse IRIS-2 adopts a helical conformation, leading to a longer alpha2 helix than in human CD59. The N-linked glycosylation site at N18 is retained in both mouse CD59B–IRIS-1 and -2. In line with previous reports, we showed that expression of CD59A is similar in liver and islets of diabetic Akita mice and WT controls (Fig. 5 *D*, *Left*), whereas CD59B is more highly expressed in islets than in liver and is significantly down-regulated in diabetic Akita mouse islets (Fig. 5 *D*, *Right*), suggesting that mouse CD59B, but not CD59A, is affected during diabetes progression. Consistent with these data, CD59B but not CD59A, is highly expressed in the mouse MIN6 pancreatic β-cell line, as compared to liver where CD59A is dominant (Fig. 5*E*). Using isoform-specific primers we showed by RT-PCR that the IRIS-1 and IRIS-2 isoforms are expressed in MIN6 cells (Fig. 5*F*). RNA was then isolated from mouse liver, spleen, and pancreatic islets. Both CD59B-IRIS isoforms were found in mouse islets (Fig. 5*G*, quantification in Fig. 5*H*) and expression of mouse IRIS-2 was down-regulated in diabetic db/db mouse islets, as compared to healthy controls (Fig. 5*I*), suggesting that this specific transcript may be down-regulated in vivo under diabetic conditions. We next investigated the function of CD59B-IRIS expression in mouse islet cells by producing CRISPR/Cas9-mediated CD59B knockout MIN6 cells. We produced clones with total CD59B knockout, as well as clones with specific knockout of canonical CD59B, but still expressing CD59B-IRIS isoforms (*SI Appendix*, Fig. S2 *A–C*). Secretion assays showed that cells lacking all CD59B isoforms did not secrete insulin upon stimulation, whereas cells lacking only canonical CD59B, but expressing IRIS-1/2, retained normal levels of insulin secretion, demonstrating that IRIS-1/2 are also necessary and sufficient for insulin exocytosis in mouse β-cells (Fig. 5*J*). To verify this, mouse CD59B–IRIS-1 and –IRIS-2 were reexpressed in total CD59B KO MIN6 cells, rescuing insulin secretion in these cells (Fig. 5*K*).

Discussion

CD59 is a ubiquitously expressed GPI-anchored protein found at high levels at the cell surface, where it protects cells against lysis by the membrane attack complex of complement. We previously showed that non–GPI-anchored CD59 can be transported from the endoplasmic reticulum (ER) into the cytosol in an N-linked glycosylation-dependent manner, where it interacts with components of insulin exocytotic machinery and allows for hormone secretion (7). In the current paper, we identify at both RNA and protein levels the existence of endogenous non–GPI-anchored CD59 splice variant isoforms, IRIS-1 and IRIS-2, that fulfill this role in cells of human pancreatic islets. While there are several described CD59 transcripts predicted to encode a protein product, these are the only two that differ in their amino acid sequence and that do not encode a predicted GPI-anchor signal peptide at the C terminus. We found that each of the two CD59-IRIS isoforms permit different phases of insulin release. IRIS-1 and -2 each share identical N-terminal homology to canonical CD59, including the N-terminal signal peptide that is removed in the ER, and the N-linked glycosylation site that we previously identified as required for retrotranslocation from the ER to the cytosol. However, the IRIS isoforms have unique C-terminal domains, which may provide differential localization or differential functions within insulin secretion. For instance, a larger proportion of total IRIS-2 was found in the membrane/organelle fraction, and this may be due to interactions of the C-terminal domain or extended loop with membrane-associated ligands. An electropositive patch was also found in the C-terminal region of human IRIS-1, suggesting possible interactions with DNA and consistent with immunostaining of this specific isoform within islet cell nuclei. This patch is not found on the structure of canonical CD59. It is therefore possible that the unique C-terminal sequences of each of the isoforms mediate additional interactions to convey intracellular functions or properties in addition to direct involvement in insulin secretion. We believe that the localization of IRIS-1 in the nuclei and cytoplasm of β-cells has different

Downloaded from https://www.pnas.org by Uppsala Universitetsbibliotek on September 22, 2022 from IP address 130.238.191.184.

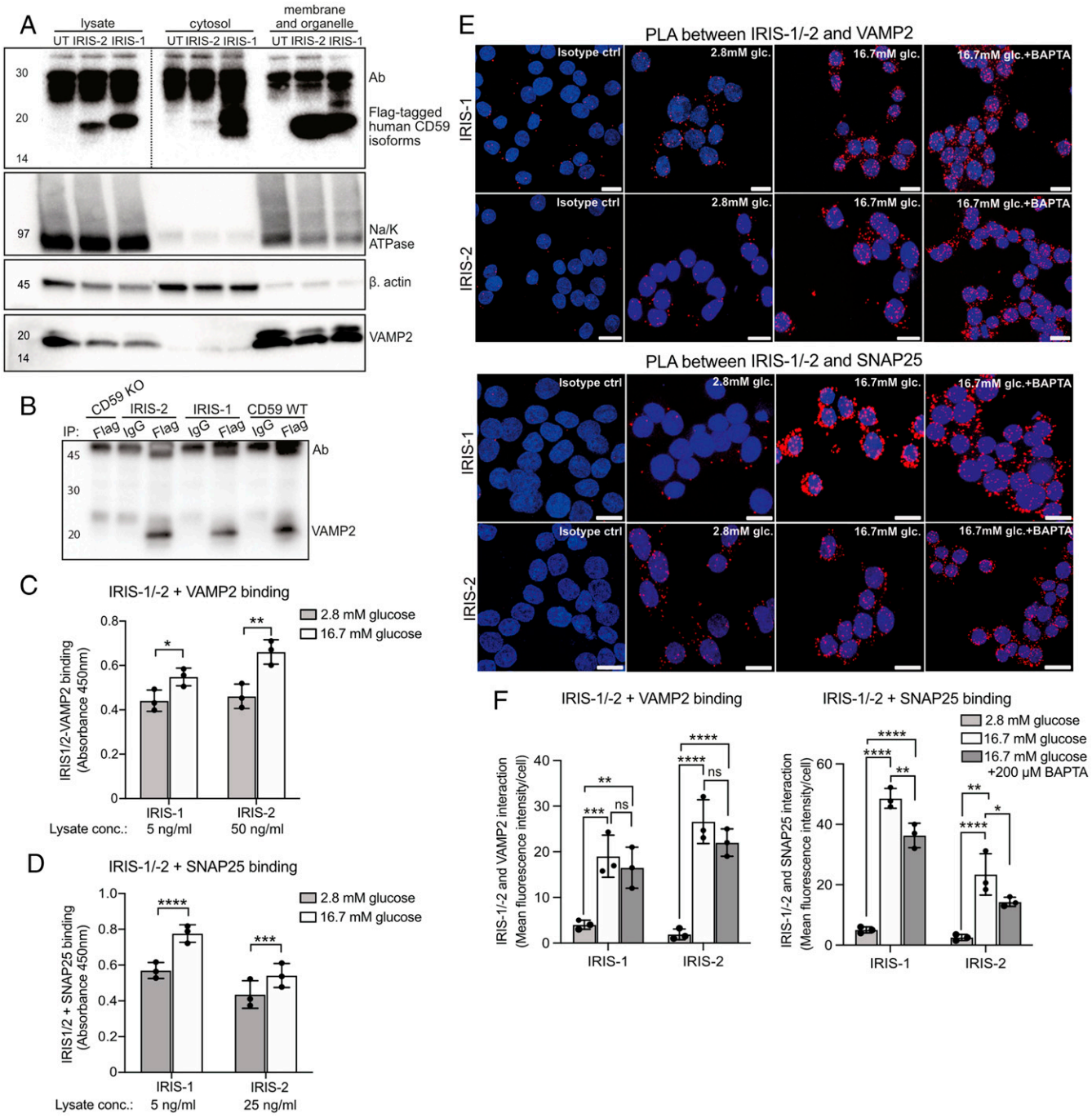

Fig. 4. (*A*) Western blot representing subcellular fractionation of INS-1 CD59-KO cells overexpressing FLAG-tagged human IRIS-1 and IRIS-2. Control proteins were found in expected compartments; $n = 5$ biological repeats. (*B*) Coimmunoprecipitation of IRIS-1, IRIS-2, and WT CD59 with VAMP2 from INS-1 CD59-KO cells stably expressing FLAG-tagged CD59 isoforms; $n = 4$ biological repeats. ELISA was used to verify the interaction between IRIS-1, IRIS-2, and VAMP2 (*C*) or SNAP25 (*D*) in lysates from INS-1 CD59-KO cells stably overexpressing IRIS-1 or IRIS-2. Prior to ELISA, cells were incubated with either high (16.7 mM) or low (2.8 mM) glucose concentrations; $n = 3$ biological repeats. Background absorbance values obtained for negative control (lysates of INS-1 CD59-KO cells) were subtracted from the presented samples. (*E*) Proximity ligation assay was used to assess colocalization (red dots) of CD59 isoforms with VAMP2 or SNAP25, under low or high glucose conditions, and in the presence of the calcium chelator BAPTA-AM. (*F*) Quantification of interactions shown in *E*; $n = 3$ biologial repeats. Statistics (in *C* and *D*): two-way ANOVA with Sidak's posttest; (*F*): two-way ANOVA with Bonferroni's posttest. Error bars indicate SD. $^{*}P < 0.05$, $^{**}P < 0.01$, $^{***}P < 0.001$, and $^{****}P < 0.0001$.

functional consequences, and that nuclear IRIS-1 does not contradict the role of IRIS-1 in the cytosol, which is interaction with SNARE proteins and enhancement of insulin secretion. Insulin resistance combined with decreased insulin release, leading to hyperglycemia, are characteristic for T2D. Additionally, one of the earliest manifestations of T2D is a selective loss of first phase of insulin secretion (9). We have shown that IRIS-1 stimulates the first phase of insulin release in INS-1 cells, and that both isoforms rescue insulin secretion in cells lacking endogenous CD59 expression. Expression of both IRIS-1 and IRIS-2 are down-regulated in primary human pancreatic islets from T2D patients, compared to healthy individuals. Moreover, glucotoxicity induced in primary, healthy human islets led to a significant decrease of IRIS-1 expression, suggesting that prolonged high glucose levels leading to decreased expression of IRIS-1 could be an important factor in the development of T2D. IRIS-1 from human pancreatic islets

Downloaded from https://www.pnas.org by Uppsala Universitetsbibliotek on September 22, 2022 from IP address 130.238.191.184.

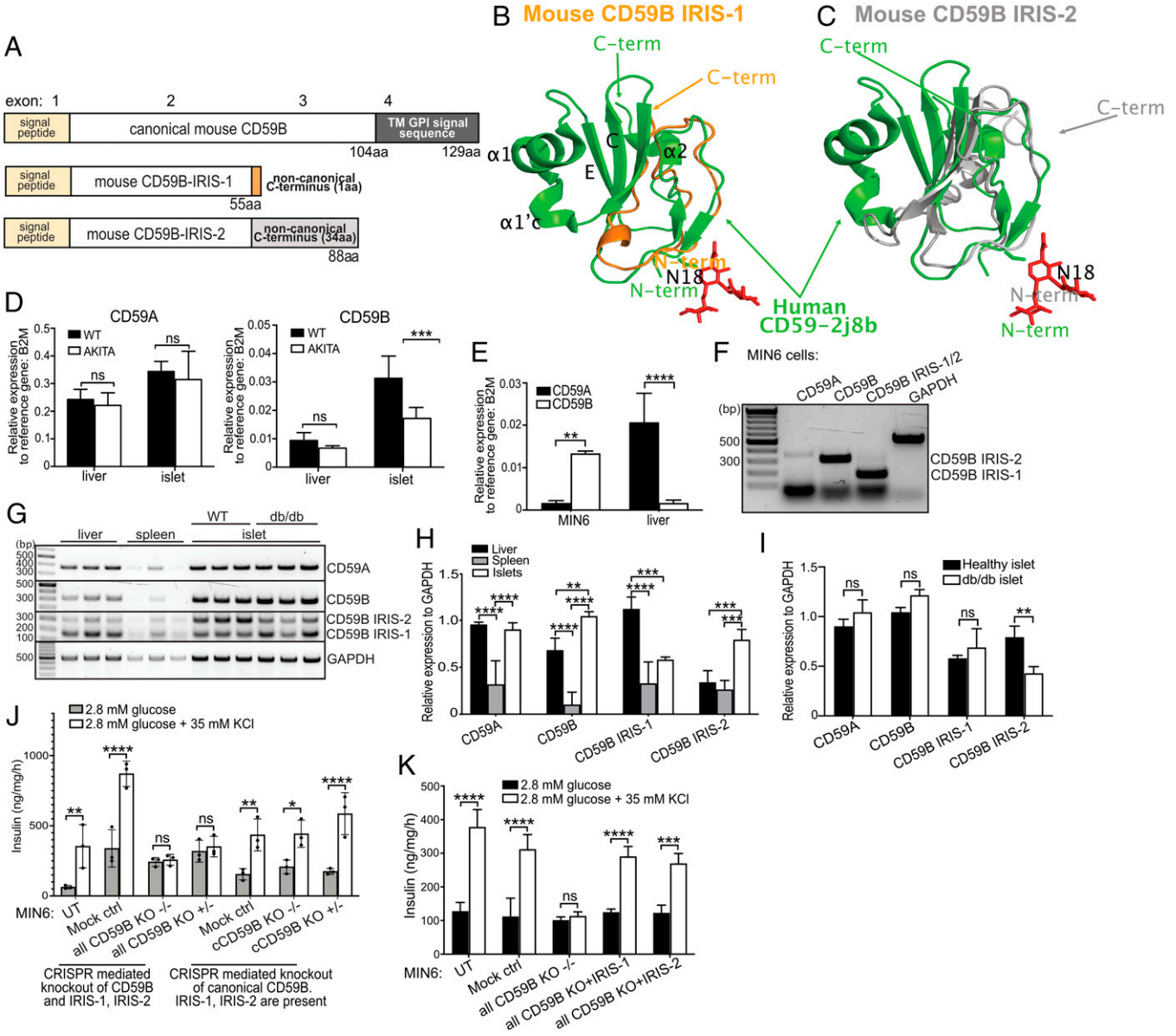

Fig. 5. (*A*) Scheme of alternative splice variants of mouse CD59B, lacking the GPI-anchoring domain with C-terminal domains (of 1 amino acid [aa] and 34 aa for IRIS-1 and -2, respectively). These isoforms were named mouse IRIS-1 and IRIS-2 (Mouse Isoforms Rescuing Insulin Secretion 1 and 2). The 3D structure of human CD59 (green) superimposed onto mouse IRIS-1 (orange) (*B*), and IRIS-2 (gray) (*C*). The *N*-glycan at N18 is marked in red. The orientation of mouse IRIS-1 and IRIS-2 is slightly shifted as compared to Fig. 1 *B–D* to visualize the C-terminal regions. In the short mouse IRIS-1 model, helices alpha1 and alpha1′c and strands *E* and *C* are missing as compared to the human CD59 experimental structure. In the predicted mouse IRIS-2 structure, helices alpha1, alpha1′c, and strand *E* are missing as compared to human CD59. (*D*) CD59A expression (*Left*) and CD59B expression (*Right*) in WT and diabetic Akita mice liver and pancreatic islets, measured by qPCR; $n = 3$ technical repeats. (*E*) Expression of CD59A and CD59B in the mouse pancreatic β-cell line (MIN6) and mouse liver; $n = 3$ biological repeats. (*F*) Mouse CD59B isoforms in MIN6 cells detected by RT-PCR; $n = 3$ biological repeats. (*G*) RT-PCR results showing expression of mouse IRIS-1 and IRIS-2 in liver, spleen, and islets isolated from WT and diabetic db/db mice; $n = 3$ technical repeats. (*H*) Quantification of WT results shown in panel *G*. (*I*) Quantification of IRIS-1 and IRIS-2 in diabetic db/db mouse and WT islets shown in panel *G*. (*J*) K^+ stimulated insulin secretion performed on MIN6 cells, MIN6 with total CD59B knockout, or MIN6 with targeted knockout of canonical CD59B (cCD59B) only, leaving IRIS-1 and IRIS-2 still expressed. Heterozygous knockouts: $^{+/-}$; homozygous knockouts: $^{-/-}$; $n = 5$ biological repeats. (*K*) Reexpression of mouse IRIS-1 or IRIS-2 in MIN6 cells with total CD59B KO restores K^+-stimulated insulin secretion; $n = 4$ biological repeats. Statistics (in *D*, *E*, and *H–K*): two-way ANOVA with Bonferroni's posttest. Error bars indicate SD. *$P < 0.05$, **$P < 0.01$, ***$P < 0.001$, and ****$P < 0.0001$.

was deglycosylated, in contrast to glycosylated human IRIS-1 overexpressed in INS-1 cells. In our experiments we used INS-1 cells with CRISPR/Cas9-mediated knockout of CD59. To stimulate insulin secretion, two different secretagogues were used: high glucose (16.7 mM) and depolarizing potassium (35 mM) concentrations. Glucose undergoes metabolism in mitochondria, and depolarizing concentrations of potassium bypass metabolism and activate voltage-gated calcium channels, triggering exocytosis. In the CD59-KO cells, insulin secretion was strongly reduced in response to glucose, but not potassium stimulation, indicating that CD59 may also be involved upstream of membrane depolarization, in glucose metabolism. An increase in basal secretion in CD59-KO INS-1 and MIN6 cells was also seen, and not affected by diazoxide, suggesting that insulin may be missorted to the constitutive pathway when CD59 is absent. We also identified similar non–GPI-anchored isoforms of mouse *Cd59b*, which itself has tissue-limited expression patterns (8), suggesting a specialized function compared to the ubiquitously expressed *Cd59a*. In islets from diabetic Akita mice, *Cd59b* expression levels were significantly reduced, possibly due to the loss of β-cells

Downloaded from https://www.pnas.org by Uppsala Universitetsbibliotek on September 22, 2022 from IP address 130.238.191.184.

in these mice, which harbor a mutation in the Ins2 gene, leading to insulin misfolding and β-cell apoptosis (10). This also suggests an enrichment of *CD59b* expression in the β-cell compartment of the islet. The non–GPI-anchored CD59-IRIS isoforms also showed altered expression patterns in islets of db/db mice, a hyperphagic model of obesity-induced diabetes. Given that incubation of human islets with high glucose led to down-regulation of human CD59-IRIS expression, further study of the temporal changes of CD59-IRIS isoforms in islets of different mouse models could help elucidate the in vivo factors that regulate their expression. The reported expression patterns of mouse *CD59b* may also point to other tissue or cell types where CD59-IRIS may also play a role in regulated exocytosis. Similar CD59-IRIS isoforms most likely exist in other species. The final protein-coding exon of human CD59–IRIS-1 is found within *C11orf91*, which is highly conserved and found adjacent to the CD59 gene across mammalian species, suggesting the existence of a conserved CD59–IRIS-1 homolog. It was recently described that CD59 exists only as a pseudogene in guinea pigs, due to the lack of any encoded C-terminal GPI-anchor signal peptide, no detectable cell-surface expression, and low or undetectable transcription levels in tested tissues (11); but our findings suggest that a tissue-restricted expression of the non–GPI-anchored guinea pig CD59 protein should be investigated for functions in insulin secretion. This would suggest that, in the guinea pig, only the secretory rather than complement inhibitory function of *Cd59* may have been evolutionarily conserved. These data open a path for future studies into CD59-IRIS expression and function, such as identification of the additional specific CD59-IRIS binding partners within the cell, which could provide new therapeutic targets for enhancement of insulin secretion in T2D.

Materials and Methods

Human Islet Donors. Deidentified isolated pancreatic islets from human donors were obtained from the Nordic Network for Islet Transplantation (Uppsala University, Sweden), under approval of the ethics committees at Uppsala and Lund universities.

Animal Models. Rat and mice use was approved by the Malmo/Lund Animal Care and Use Committee (permits M9-15 and M87-14, 20069/2020).

INS-1 832/13 cells. INS-1 832/13 cells (a gift from C. Newgard, Duke University, Durham, NC) (12) were cultured in supplemented RPMI medium 1640 (detailed medium composition is provided in *SI Appendix*).

MIN6 cells. MIN6 cells (a gift from J. Miyazaki, Osaka University Medical School, Osaka, Japan) (13) were cultured in supplemented low-glucose Dulbecco's modified Eagle medium (DMEM) (detailed medium composition in *SI Appendix*).

EndoC-βH1 cells. EndoC-βH1 cells (a gift from R. Scharfmann, INSERM, Paris, France) (14) were cultured in supplemented low-glucose DMEM (detailed medium composition in *SI Appendix*).

RT-PCR. RNA was extracted using an RNA purification kit (Qiagen). cDNA was synthesized using oligo-dT primers and SuperScript IV (Invitrogen) and amplicon amplified with Red-Taq (Sigma) or DreamTaq Green PCR Master mix (Thermo Scientific).

Insulin Secretion. INS-1, MIN6, and EndoC-βH1 cells were preincubated for 2 h in 2.8 mM glucose and then stimulated with 2.8 or 16.7 mM glucose or 2.8 mM glucose combined with 35 mM KCl for 1 h.

Western Blots. Cells were lysed in radio-immunoprecipitation assay lysis buffer. Proteins were resolved on SDS-PAGE gels and probed with antibodies against FLAG-tag, β-actin, β-tubulin, CD59-BRIC 229, VAMP2, IRIS-1, IRIS-2, Na/K ATPase, or antimouse IRIS-2.

Cell Fractionation. INS-1 cells were separated into cytosolic and membrane and organelle fractions according to protocol from the Mem-PER Plus kit (Thermo Scientific).

Coimmunoprecipitation. INS-1 cells were incubated in 16.7 mM glucose overnight. After lysis, an aliquot was saved as input sample. Remaining lysate was mixed (overnight) with 10 μg of FLAG-tag antibodies, or rat IgG2a isotype control bound to Sepharose protein G beads. Beads were extensively washed with lysis buffer and coprecipitated proteins were eluted.

Immunofluorescence. IRIS-1, IRIS-2, insulin, and glucagon were visualized by indirect immunocytochemistry in primary human pancreatic islets (dispersed or intact) and in INS-1 cells.

Electron Microscopy. CD59-KO INS-1 cells overexpressing human IRIS-1, or IRIS-2, were preincubated in 2.8 mM glucose for 2 h and then stimulated with 16.7 mM glucose for 10 min (IRIS-1) or overnight (IRIS-2). Primary antibodies against insulin, IRIS-1, or IRIS-2 were used, followed by the incubation with secondary antibodies with 10 nm gold particles (against insulin) and 20 nm gold particles (against IRIS isoforms). Grids were examined using a FEI Technai Biotwin 120-kV microscope.

Quantitative PCR. RNA was extracted using an RNA purification kit (Qiagen). cDNA was synthesized using oligo-dT primers and SuperScript IV (Invitrogen). Quantitative PCR was performed with specific TaqMan probes (Applied Biosystem) and the Viia7 Real-Time PCR system (Thermo Fisher).

VAMP2/SNAP25–IRIS-1/2 ELISA Detection. INS-1 CD59-KO cells overexpressing human IRIS-1 and IRIS-2, or CD59-KO cells as a negative control, were lysed after overnight incubation in 2.8 or 16.7 mM glucose. Lysate protein content was measured by bicinchoninic acid assay, and equal amounts were incubated overnight in microtiter plates coated with anti-VAMP2, anti-SNAP25, or isotype control antibodies. IRIS-1 and IRIS-2 were then detected with biotinylated antibodies followed by horseradish peroxidase-conjugated streptavidin. Absorbance was measured at 450 nm. The background absorbance from CD59-KO cell lysates were subtracted from the absorbance values of IRIS-expressing lysates to give the specific signal of detection of VAMP2- or SNAP25-IRIS interaction complexes.

Molecular Modeling. Different tools were used to develop the human and mouse protein 3D models, depending on the tasks (i.e., homology modeling, threading, simulations). In all cases, PDB files were manipulated with Python scripts available in PDB-Tools (15) and with MayaChemTools Perl scripts (16). Secondary structure predictions were carried out with the PSIPRED server (17). Sequences to 3D structure alignments were computed using the PROMALS3D server (18). Simple energy minimization computations were performed for all 3D models using Chimera utilities (19) but for some models, more advanced simulation protocols were needed (detailed informations in *SI Appendix*).

Patch-Clamp Electrophysiology. Cells were continuously superfused with an extracellular solution containing 138 mM NaCl, 5.6 mM KCl, 1.2 mM $MgCl_2$, 2.6 mM $CaCl_2$, 3 mM D-glucose, and 5 mM Hepes, pH 7.4. Voltage-dependent currents and exocytosis were measured in whole-cell voltage-clamp mode, with an intracellular solution containing 125 mM Cs-glutamate, 10 mM CsCl, 10 mM NaCl, 1 mM $MgCl_2$, 0.05 mM ethylene glycol-bis(β-aminoethyl ether)-N,N,N′,N′-tetraacetic acid, 3 mM Mg-ATP, 0.1 mM cyclic adenosine monophosphate, and 5 mM Hepes, pH 7.2.

TIRF-M Imaging. Cells were transfected with the secretory granule markers NPY-EGFP or NPY-mOrange2 (20) and imaged using a custom-built lens-type total internal reflection microscope.

Quantification and Statistical Analysis. All experiments were performed in at least three independent repeats, with at least two duplicate samples per condition in each repeat. The mean differences between groups that have been split on two independent variables were compared with two-way analysis of variance (ANOVA). Student's *t* test was used in the case of two independent group comparisons and one-way ANOVA when three or more independent groups were compared. Data lacking normal distribution were analyzed using a nonparametric Mann–Whitney test. The Bonferroni, Sidak, and Dunnett tests were used in the case of multiple comparisons. In all figures, $*P < 0.05$, $**P < 0.01$, $***P < 0.001$, and $****P < 0.0001$.

Data Availability. All study data are included in the article and/or *SI Appendix*.

Downloaded from https://www.pnas.org by Uppsala Universitetsbibliotek on September 22, 2022 from IP address 130.238.191.184.

ACKNOWLEDGMENTS. We thank Dr. Estefania Torres-Vega for help in optimizing the immunofluorescence staining of human islets, Docent Yvonne Ceder for providing RNA from human tissues, Sofie Ingvast for providing the human pancreatic islets samples, Prof. Lena Eliasson for scientific advice regarding electron microscopy data calculation, and Dr. Jonathan Esguerra for bioinformatic assistance. This study was supported by the Novo Nordisk Foundation Distinguished Investigator Grant NNF20OC0059476, the Knut and Alice Wallenberg Foundation, the Swedish Research Council, Strategic Research Area Exodiab, Dnr 2009-1039, the Novo Nordisk Fundation Grant NNF20OC0063600, the Swedish Research Council Grant 2019-01415, the Hjelt Diabetes Foundation, the Crafoord Foundation, and the Albert Påhlsson Foundation. Maciej Noga and Katarzyna Wozniak are students of Biotechnology at Rzeszow University, Poland.

Author affiliations: [a]Section of Medical Protein Chemistry, Department of Translational Medicine, Lund University, 214-28 Malmö, Sweden; [b]Department of Medical Cell Biology, Uppsala University, BMC 571, 75123 Uppsala, Sweden; [c]Université Paris Cité, Department of Neuroscience, NeuroDiderot, Inserm U1141, Paris, F-75019 France; [d]Lund University Diabetes Centre, Department of Clinical Sciences Malmö, Lund University, 214-28 Malmö, Sweden; and [e]Department of Immunology, Genetics, and Pathology, Uppsala University, 751 85 Uppsala, Sweden

1. B. Ghebrehiwet, The complement system: An evolution in progress. *F1000 Res.* **5**, 2840 (2016).
2. J. V. Sarma, P. A. Ward, The complement system. *Cell Tissue Res.* **343**, 227–235 (2011).
3. L. L. Gonzalez, K. Garrie, M. D. Turner, Type 2 diabetes: An autoinflammatory disease driven by metabolic stress. *Biochim. Biophys. Acta Mol. Basis Dis.* **1864**, 3805–3823 (2018).
4. B. C. King, A. M. Blom, Complement in metabolic disease: Metaflammation and a two-edged sword. *Semin. Immunopathol.* **43**, 829–841 10.1007/s00281-021-00873-w. (2021).
5. K. J. Leath *et al.*, High-resolution structures of bacterially expressed soluble human CD59. *Acta Crystallogr. Sect. F Struct. Biol. Cryst. Commun.* **63**, 648–652 (2007).
6. U. Krus *et al.*, The complement inhibitor CD59 regulates insulin secretion by modulating exocytotic events. Cell Metabolism **19**, 883–890 (2014).
7. E. Golec *et al.*, A cryptic non-GPI-anchored cytosolic isoform of CD59 controls insulin exocytosis in pancreatic β-cells by interaction with SNARE proteins. *FASEB J.* **33**, 12425–12434 (2019).
8. C. L. Harris *et al.*, Characterization of the mouse analogues of CD59 using novel monoclonal antibodies: Tissue distribution and functional comparison. *Immunology* **109**, 117–126 (2003).
9. E. Cerasi, S. Ependić, R. Luft, Dose-response relation between plasma-insulin and blood-glucose levels during oral glucose loads in prediabetic and diabetic subjects. *Lancet* **1**, 794–797 (1973).
10. C. E. Mathews, S. H. Langley, E. H. Leiter, New mouse model to study islet transplantation in insulin-dependent diabetes mellitus. *Transplantation* **73**, 1333–1336 (2002).
11. H. Boshra, W. M. Zelek, T. R. Hughes, S. Rodriguez de Cordoba, B. P. Morgan, Absence of CD59 in Guinea Pigs: Analysis of the *Cavia porcellus* Genome Suggests the Evolution of a *CD59* Pseudogene. *J. Immunol.* **200**, 327–335 (2018).
12. H. E. Hohmeier *et al.*, Isolation of INS-1-derived cell lines with robust ATP-sensitive K+ channel-dependent and -independent glucose-stimulated insulin secretion. *Diabetes* **49**, 424–430 (2000).
13. J. Miyazaki *et al.*, Establishment of a pancreatic beta cell line that retains glucose-inducible insulin secretion: Special reference to expression of glucose transporter isoforms. *Endocrinology* **127**, 126–132 (1990).
14. P. Ravassard *et al.*, A genetically engineered human pancreatic β cell line exhibiting glucose-inducible insulin secretion. *J. Clin. Invest.* **121**, 3589–3597 (2011).
15. J. P. G. L. M. Rodrigues, J. M. C. Teixeira, M. Trellet, A. M. J. J. Bonvin, pdb-tools: A swiss army knife for molecular structures. *F1000 Res.* **7**, 1961 (2018).
16. M. Sud, MayaChemTools: An Open Source Package for Computational Drug Discovery. *J. Chem. Inf. Model.* **56**, 2292–2297 (2016).
17. D. W. A. Buchan, D. T. Jones, The PSIPRED Protein Analysis Workbench: 20 years on. *Nucleic Acids Res.* **47** (W1), W402–W407 (2019).
18. J. Pei, B. H. Kim, N. V. Grishin, PROMALS3D: A tool for multiple protein sequence and structure alignments. *Nucleic Acids Res.* **36**, 2295–2300 (2008).
19. E. F. Pettersen *et al.*, UCSF Chimera–a visualization system for exploratory research and analysis. *J. Comput. Chem.* **25**, 1605–1612 (2004).
20. N. R. Gandasi *et al.*, Survey of Red Fluorescence Proteins as Markers for Secretory Granule Exocytosis. *PLoS One* **10**, e0127801 (2015).

Downloaded from https://www.pnas.org by Uppsala Universitetsbibliotek on September 22, 2022 from IP address 130.238.191.184.